Published in IET Microwaves, Antennas & Propagation
Received on 25th July 2014
Revised on 24th September 2014
Accepted on 3rd October 2014
doi: 10.1049/iet-map.2014.0490

ISSN 1751-8725

Loading metamaterial perfect absorber method for in-band radar cross section reduction based on the surface current distribution of array antennas

Si-Jia Li, Jun Gao, Xiang-Yu Cao, Yi Zhao, Zhao Zhang, Hong-Xi Liu

Information and Navigation College, Air Force Engineering University, No. 1, Fenghao East Road, Lianhu Zone, Xi'an 710077, People's Republic of China
E-mail: lsj051@126.com

Abstract: A loading metamaterial perfect absorber (MPA) method is proposed to reduce the in-band radar cross section (RCS) and preserve the radiation characters for the guidewave slot array antennas in this study. The surface current distributions of the array antennas are divided into the strong current area and the weak current area. The metal surface with the strong current is retained to avoid the radiation deterioration, and the MPA is only loaded on the weak current area by the three layers MPA for RCS reduction. The RCS of a 1×10 guidewave slot array antennas is reduced using the method. Simulated S_{11}, radiation patterns, gain and RCS reduction of the array antennas are compared with measured results. Experimental results indicated that the in-band RCS of the array antennas loading the MPA has dramatically reduced with only about 0.73 dB gain reduction and the RCS reduction are not significant in out-of-band while the radiation characters is unchanged. The experimental results are in good agreement with the numerical simulations.

1 Introduction

Nowadays, it has been a topic of immense strategic interest to reduce the radar cross section (RCS) of an antenna without compromising its radiation characteristics. For out-of-band frequencies, it is well known that the RCS of antenna/array can be significantly reduced by placing the periodic resistive surface [1, 2] and the suitably shaped band-pass radome, such as frequency selective surfaces (FSS) [3]. However, when the radome is transparent, no RCS reduction of the antenna will significantly take place for in-band frequency.

As an excellent candidate, the metamaterial absorber has been paid attention to for in-band RCS reduction. In [4], the application of electromagnetic bandgap (EBG) radar absorbing material loaded with lumped resistances to ridged waveguide slot array antennas to reduce its in-band RCS was investigated, in which the lumped resistive elements were used to better match the impedance of free space, and as the chief contributor of absorption. The designed idea is different from this work in [4]. In [5], an artificial magnetic conductor (AMC) and perfect electric conductor (PEC) surface were combined together for in-band RCS reduction and radiation improvement of waveguide slot antenna based on the principle of passive cancellation. In [6], two different AMCs were analysed for ultra-thin and broadband RAM design. In [7], the reflection characteristic of a composite planar AMC surface has been investigated and fabricated for broadband RCS reduction. Similarly, a broadband RCS reduction for a waveguide slot antenna with an orthogonal array of CSRR-AMC is presented in [8]. However, it is obvious that the RCS is evidently reduced in boresight direction but increased in other directions in [5–8]. Recently, the metamaterial perfect absorber (MPA) with ultrathin structure and near-unity absorptivity was firstly demonstrated by Landy *et al.* in 2008, which has become an important aspect in the research of metamaterials [9–17]. In 2013, an MPA with polarisation-insensitive and wide-angle absorption was presented for in-band RCS reduction of waveguide slot antenna in [12]. The maximum absorptivity of this absorber is 99.8% with a full width at half maximum (FWHM) of 220 MHz. Then, a novel MPA structure is applied for in-band RCS reduction of a circularly polarised tilted beam antenna in [13]. However, the loading MPA method cannot directly use for the guidewave slot array antennas because of the gain reduction.

In this paper, a loading MPA method that the MPA is only loaded on the weak surface current area is presented and investigated to avoid the radiation property deterioration and reduce the in-band RCS of array antennas. The loading MPA method based on a three layers MPA, which shows that the polarisation-insensitive and angular stability of the MPA are achieved, is studied and the absorbing mechanism is also analysed. The three layers MPA is demonstrated and proposed to enhance the absorption bandwidth compared the single layer MPA. The performances of the loading MPA method are illuminated by simulations and measurements for a waveguide slot array antennas.

© The Institution of Engineering and Technology 2015

2 Three layers MPA design

To reduce the in-band RCS of the guidewave slot array antennas, the three layers MPA is proposed because its absorption bandwidth satisfies the bandwidth of the array antennas. Fig. 1*a* shows the geometry of the three layers MPA, which composed of three metal square loops and a metal ground. Compared to the symmetrical structures such as circle loop, hexagonal loop, octagonal loop and dodecagonal loop, the area of square loop is more than others on the same substrate. The miniaturised and ultrathin microstructure of three layers MPA is the obvious advantage. In addition, the flexibleness and realisableness for the proposed MPA are much more than others. Every two adjacent metal sheets are separated by the dielectric substrate in Fig. 1*a*. The metal is copper with a conductivity of 5.8×10^7 S/m. FR4 is used as the three substrates ($\varepsilon_r = 4.4$, tan $\delta = 0.02$). Every metal square loop and its underlying FR4 layer compose a metamaterial layer, which may be treated as a uniform layer. The absorber is simulated and optimised using a high frequency structure simulator (HFSS 14.0) by considering a unit cell. The transmission is zero ($T = 0$) due to the copper ground plate without patterning in the bottom layer. The absorptivity (A) is defined as [9, 13, 14]

$$A = 1 - R = 1 - |S_{11}|^2 \tag{1}$$

For the three layers MPA, the free-space reflection coefficient of the MPA cell at normal incidence is given by

$$R = [z_{\text{eff}}(\omega) - \eta_0]/[z_{\text{eff}}(\omega) + \eta_0] \tag{2}$$

where the η_0 represents the impedance of free space and is approximately 377 Ω. $z_{\text{eff}}(\omega)$ is the effective impedance of the MPA cell, which includes the surface impedance to achieve large resonant dissipation and the substrate impedance because of the high tangent. By substitution of (2) in (1), the A can be written by

$$A = \frac{2\eta_0}{\text{Re}[z_{\text{eff}}(\omega)] + i \cdot \text{Im}[z_{\text{eff}}(\omega)] + \eta_0} \tag{3}$$

where Re[$z_{\text{eff}}(\omega)$] and Im[$z_{\text{eff}}(\omega)$] are, respectively, the real part and the imaginary part of $z_{\text{eff}}(\omega)$. The idea is to make the impedance of absorber match to that of the free space ($z_{\text{eff}}(\omega) = \eta_0$) and possess a large imaginary part of refraction index $n(\omega)$ simultaneously

$$z_{\text{eff}}(\omega) = \left[\mu(\omega)/\varepsilon(\omega)\right]^{0.5} \tag{4}$$

$$n_{\text{eff}}(\omega) = \left[\mu(\omega)\varepsilon(\omega)\right]^{0.5} \tag{5}$$

Therefore both the transmission and reflection are both minimised because of the impedance matching and large losses in the absorber and the incident energy will be converted into heat. At the resonant modes, the absorptivity achieved 100% for the MPA. From the expression of (3), we know that when $A = 1$, Re[$z_{\text{eff}}(\omega)$] and Im[$z_{\text{eff}}(\omega)$] can be calculated as

$$\text{Re}[z_{\text{eff}}(\omega)] = 377\,\Omega, \qquad \text{Im}[z_{\text{eff}}(\omega)] = 0 \tag{6}$$

The optimised absorptivity is given in Fig. 1*b*. From Fig. 1*b*, we can see that the frequency range with absorptivity larger than 90% is ranging from 3.14 to 3.24 GHz with a FWHM of 170 MHz (3.1–3.27 GHz). The simulated real and imaginary parts of the effective impedance of the proposed three layers MPA are given in Fig. 1*c*. It is found that the absorptivity is close to 100%, when the real part and the imaginary part of the effective impedance are, respectively, close to 377 Ω and 0.

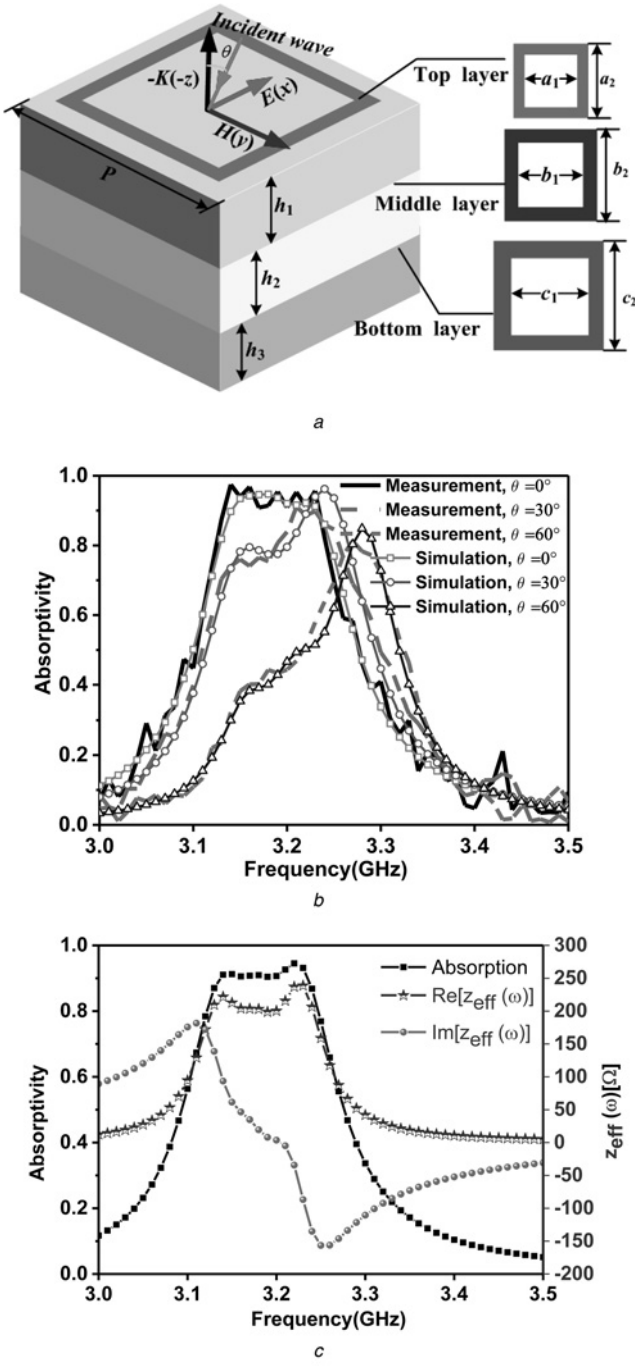

Fig. 1 *Geometry and absorptivity of the three layers MPA*

Optimised parameters are: $h_1 = h_2 = h_3 = 0.3$, $p = 15$, $a_1 = 10.52$, $a_2 = 14.1$, $b_1 = 9.58$, $b_2 = 14.14$, $c_1 = 9.22$ and $c_2 = 14.3$ (units: mm)

a Geometry of the MPA

b Simulated and measured absorptivity of the proposed MPA with the optimised geometries parameters at the incident angle of 0°, 30° and 60°

c Real part and imaginary part of the effective impedance for three layers MPA at the incident angle of 0°

© The Institution of Engineering and Technology 2015

doi: 10.1049/iet-map.2014.0490

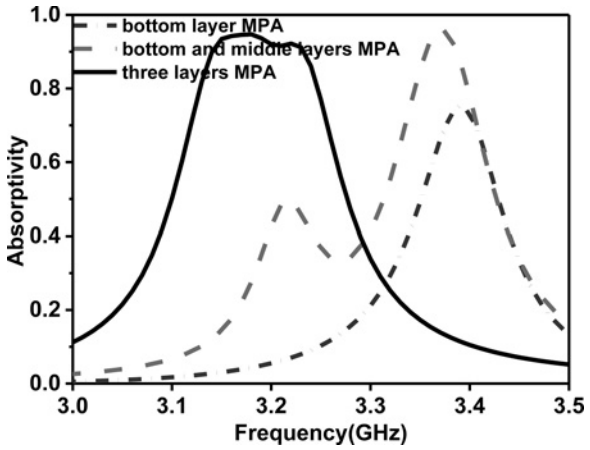

Fig. 2 *Absorptivity of the bottom layer MPA, bottom and middle layers MPA and three layers MPA*

The absorption bandwidth of the proposed MPA is increased by using the three layers MPA structures which can support three resonant modes. The resonance frequencies could be close to each other by slightly different lengths of the square loops in different layers. By tuning the parameters (a_1, a_2, b_1, b_2, c_1 and c_2), the multi-layer structure can be impedance-matched to the free space at each resonant frequency. The absorptivity peaks will decrease as the incident angle θ increase from 0° to 60°, because the MPA cannot absorb the electromagnetic wave when it is paralleled along the *xoy*-plane. The absorber obtains the absorption above 90% from 3.14 GHz to 3.24 GHz. The absorption near to zero in the range of $f < 3$ GHz or $f > 3.4$ GHz in Fig. 1*b*. The f represents the frequency of MPA.

To better understand the physical mechanism of three layers MPA, the absorption and current distributions on the three metal square loops at responses frequencies of 3.14, 3.18 and 3.22 GHz are demonstrated in Figs. 2 and 3. The coupling between the top, middle and bottom layer is very strong compared the absorptivity of the bottom layer MPA and double (bottom and middle) layers MPA. The bottom layer MPA obtains the peak of 0.75 at 3.39 GHz. The bottom and middle layers MPA achieve the peaks of 0.96 and 0.51 at 3.37 and 3.22 GHz, respectively. It concluded that the coupling between different layers is important for proposed MPA design. From Fig. 3, the current distributions of bottom and top metal square loops are strong at 3.14 GHz. The current distributions of top and middle metal square loops are strong at 3.18 GHz. At 3.22 GHz, the current distributions of top and bottom metal square loops are strong. Therefore the three metal square loops structure is the key of absorption above 90% from 3.14 to 3.24 GHz. The parameters such as a_1, a_2, b_1, b_2, c_1 and c_2 of the three layers MPA is important for the strong coupling in the process of the three layer MPA design.

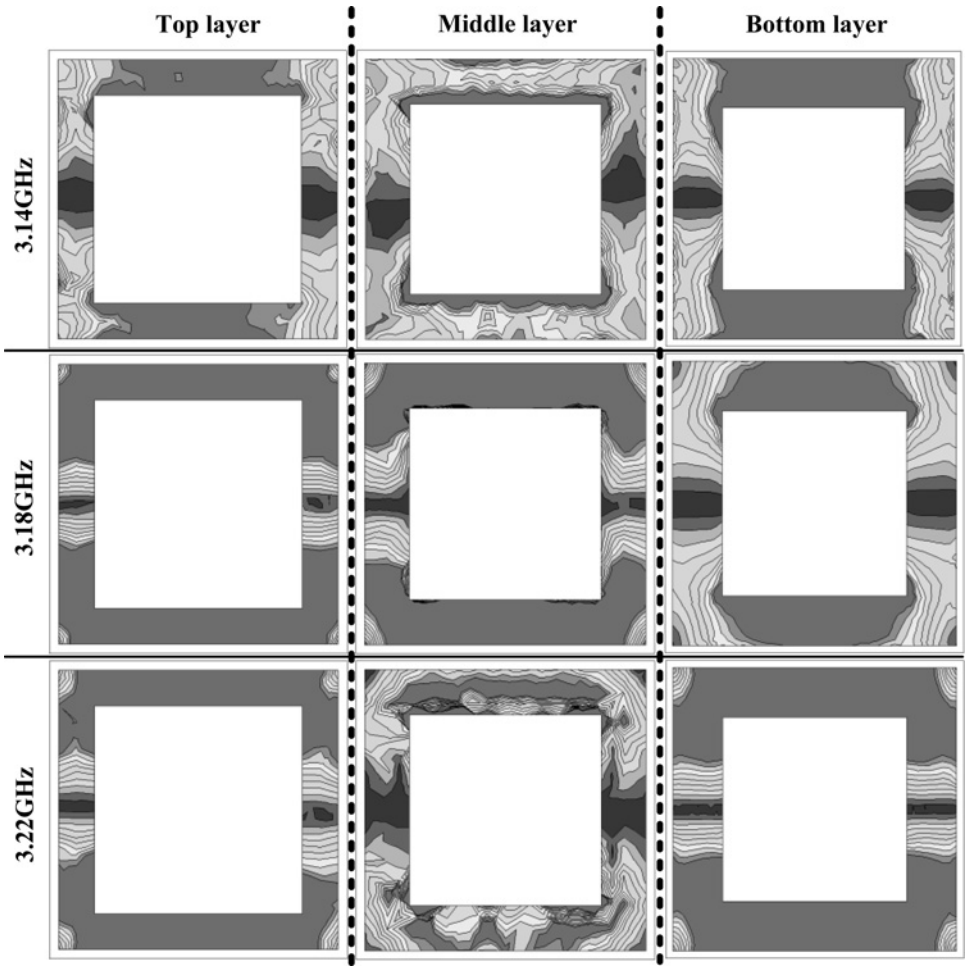

Fig. 3 *Current distributions on the three metal square loops at responses frequencies of 3.14, 3.18 and 3.22 GHz*

© The Institution of Engineering and Technology 2015

3 Loading MPA method and simulated validation

The loading MPA method mainly includes three steps. The first is to analyse the surface current distribution of the array antennas. The second is that the surface current distribution is divided into the strong current area and the weak current area. The metal surface with the strong current is retained to avoid the radiation deterioration. And simultaneously, the MPA has been loaded on the weak current area of the array for RCS reduction. The last is to optimise the distance (***L***) between the proposed MPA and the slots of the array antennas according to minimise the gain deterioration of antennas.

The geometry and its surface current distribution of the 1 × 10 guidewave slot array antennas are shown in Fig. 4. The position of feed point is in the centre of the array in Fig. 4*c*. Hence, the strong surface current area of the array antennas is near the two sides of a slot and the weak surface current is around the edge of the array antennas from Fig. 4*e*. So the MPA is loaded on the weak current area, which are given in Fig. 5*b* and the strong surface current area is retained for the array radiation. The distance ***L*** between the slot and the metamaterial absorber is optimised from 1 to 5 mm to minimise the gain deterioration, and the optimised result is 3 mm.

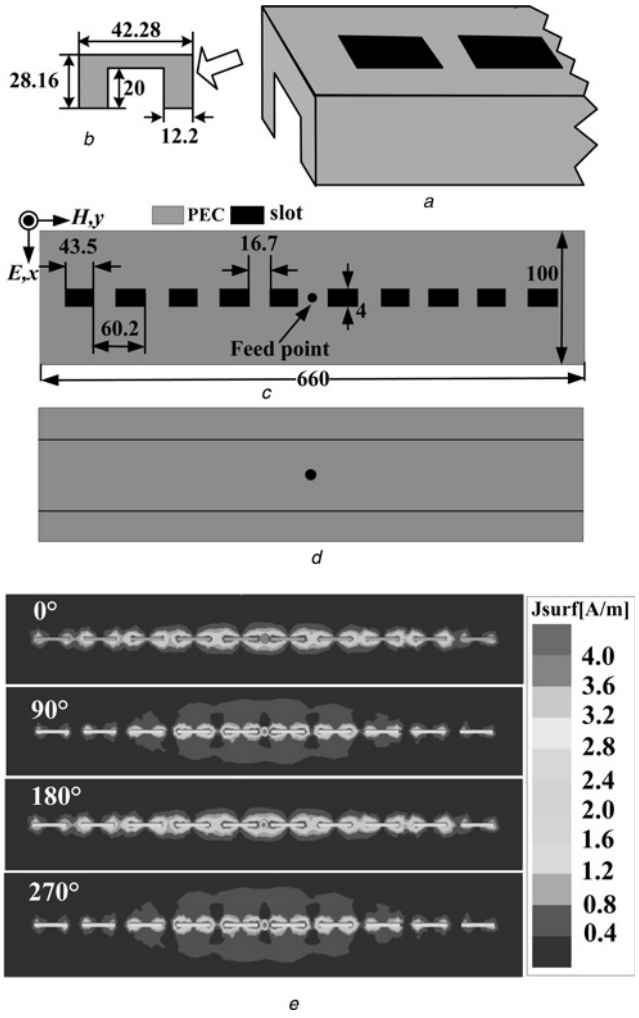

Fig. 4 *Geometry and the surface current distribution of the 1 × 10 guidewave slot array antennas (units: mm)*

a Geometry of array antennas
b Side view
c Top view for the array antennas
d Bottom view for the array antennas
e Surface current distributions of the 1 × 10 guidewave slot array antennas at 0°, 90°, 180° and 270°

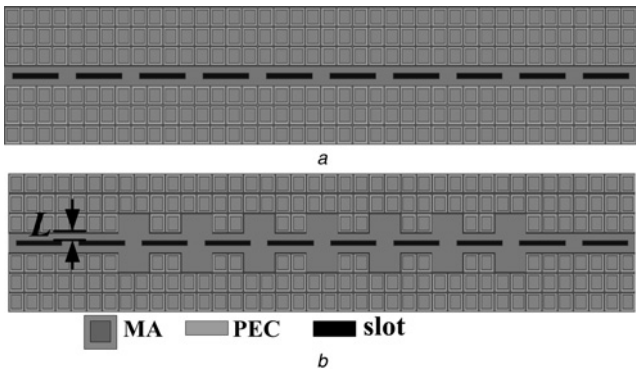

Fig. 5 *Guidewave slot array antennas loading three layers MPA*

a Using the conventional loading method
b Using the method based on the surface current distribution

To demonstrate the method, an intensive simulation study is carried out using a commercial electromagnetic solver and the results are discussed. The common antennas (without loading the three layer MPA) are the 1 × 10 guidewave slot array antennas and the array antennas loading MPA in Fig. 5*b* are the array antennas loaded with the three layer MPA using the method based on the surface current distribution. Fig. 5*a* gives the common loading method that the MPA is loaded on the strong and weak surface current distribution areas of the array antenna simultaneously to further demonstrate the advantages of the proposed design. Fig. 6*a* shows the simulated S_{11} and gain. The impedance bandwidth of 2.2% ($S_{11} < -10$ dB) from 3.15 to 3.22 GHz is achieved for the common antennas and the antennas loading MPA obtain an impedance bandwidth of 2.25% from 3.15 to 3.23 GHz, from which it can be found that the two antennas have the same resonant frequency. The gain varies from 13.6 to 14.5 dBi for the two antennas at the working frequency (3.15–3.23 GHz) and is shown in Fig. 6*b*. The antennas loading MPA have a gain of 14.1 dBi, which are 0–0.68 dB lower than that of common antennas from 3.15 to 3.2 GHz and higher than that from 3.2 to 3.23 GHz. Compared to the common array antennas, the array antennas using the conventional loading method which are shown in Fig. 5*a* have a gain of 13.6 dBi, which are 0.7–1.5 dB lower than that of common antennas from 3.15 to 3.2 GHz. The gain deterioration of the antennas in Fig. 5*a* is more than that in Fig. 5*b*. Hence the loading MPA method based on the surface current distribution of the array antennas is necessary to avoid the radiation deterioration. In the out-of-band (3–3.15 GHz and 3.23–3.4 GHz), the common array antennas and antennas in Fig. 5 cannot effectively radiate electromagnetic wave because the values of S_{11} are more than −10 dB. It is necessary to note that the gain of the proposed antenna loading MPA is slightly increased in the out-of-band (3.25–3.32 GHz) compare to that of common antenna without loading MPA. There are two reasons for the phenomenon. The impedance matching is improved by loading the MPA and the radiated area is enlarged because of the height of MPA in the out-of-band of the array antennas. Simulated radiation patterns of the array antennas at 3.18 GHz are given in Fig. 7. It can be seen that the radiation patterns of the guidewave slot array antennas loading MPA are same

© The Institution of Engineering and Technology 2015

doi: 10.1049/iet-map.2014.0490

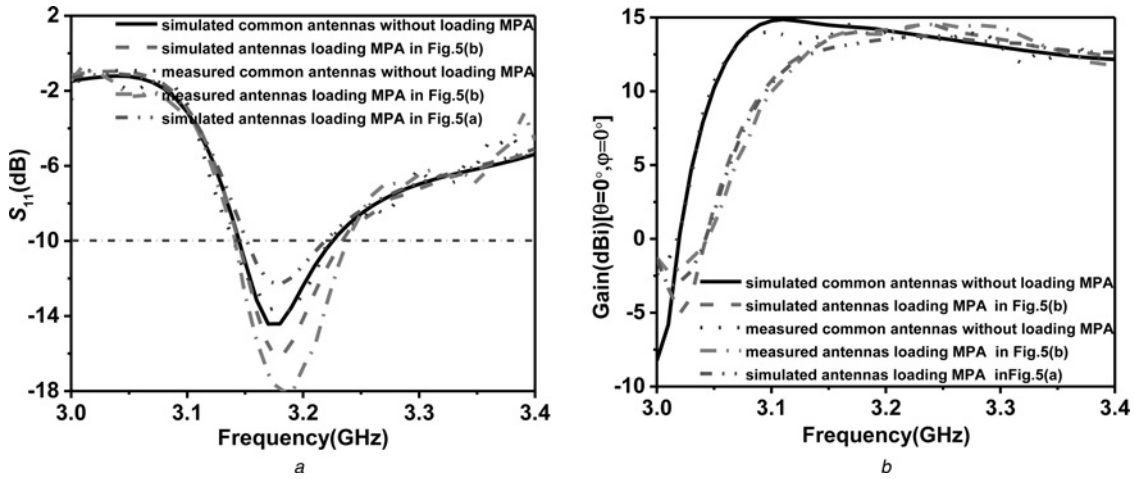

Fig. 6 *Simulated S_{11} and gain for the common guidewave slot array antennas, the antennas loading MPA in Figs. 5a and b from 3.0 to 3.4 GHz*

a S_{11}
b Gain

with common antennas at 3.18 GHz. The front-to-back ratio (FBR) remains to be better than 10.1 dB for the antennas loading MPA in Fig. 5*b*, which is 1.3 dB lower than that of common antennas. From Fig. 7, we know that the radiation characters are retained compared with the common array antennas. The S_{11} and gain remain because of the coherence of surface current for the common antennas radiation and the radiation of antennas loading MPA in Fig. 5*b* shown in Fig. 8. And radiation patterns of the antennas loading the MPA in Fig. 5*b* are retained without deterioration because of the same reason.

The monostatic in-band RCS reduction and bistatic RCSs for the guidewave slot array antennas are given in Fig. 9. From Fig. 9*a*, it is found that the in-band RCS reductions of the array antennas are significantly from 3.14 to 3.23 GHz for the *x*-polarised and *y*-polarised incident wave. In out-of-band, the RCS reductions of the array antennas loading MPA in Fig. 5*b* are not obvious and the maximum value is less than 5 dB in Figs. 9*a* and *b*. This phenomenon is illuminated by the absorption above 90% from 3.14 to 3.24 GHz for the proposed three layers MPA and the absorption will decrease in out-of-band. The RCS reduction peaks are, respectively, −12.7 dB at 3.21 GHz for *x*-polarised incident wave and −14.6 dB at 3.18 GHz for *y*-polarised incident wave. As the incident angle increased from 0° to 60°, the RCS reduction decreased from −12.7 to −8.9 dB for *x*-polarised incident wave and from −14.6 to −8.1 dB for *y*-polarised incident wave. Figs. 9*c* and *d* present the bistatic RCS for the common array antennas and the antennas loading the MPA with *x*-polarised and *y*-polarised incident waves at 3.18 GHz. From Fig. 9*c*, it can be found that in the case of the *x*-direction polarised incident wave, the RCS has been effectively reduced in angular ranges of [−110°, −50°], [−30°, 30°] and [50°, 110°] in the *xoz*-plane and [−45°, 45°] in the *yoz*-plane. From Fig. 9*d*, we find the RCS has been effectively reduced in angular ranges of [−110°, 110°] in the *xoz*-plane and [−10°, 10°] in the *yoz*-plane for the *y*-direction polarised incident wave. The RCS reduction in the *xoz*-plane for *y*-polarised incident wave is more significant

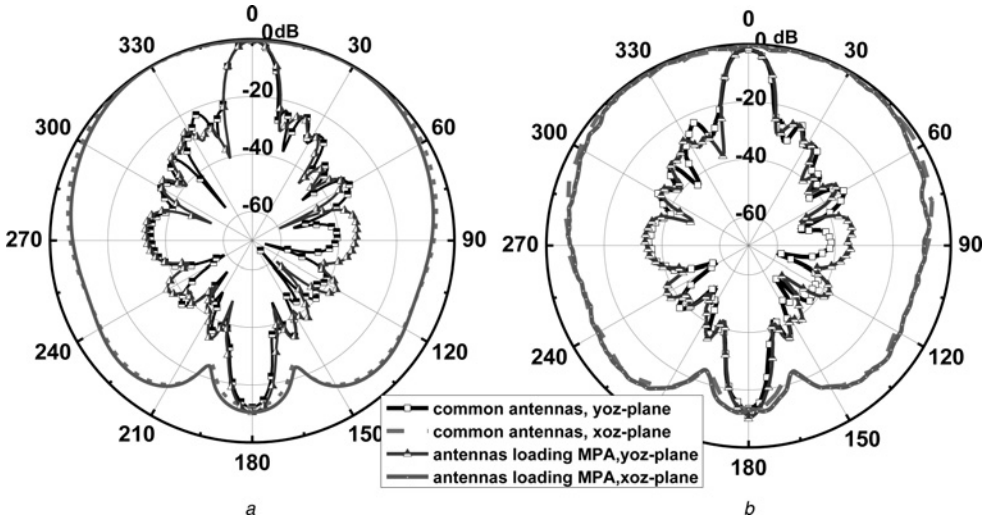

Fig. 7 *Simulated and experimental radiation patterns of the guidewave slot array antennas loading MPA in Fig. 5b and common antennas at 3.18 GHz*

a Simulated results
b Experimental results

© The Institution of Engineering and Technology 2015

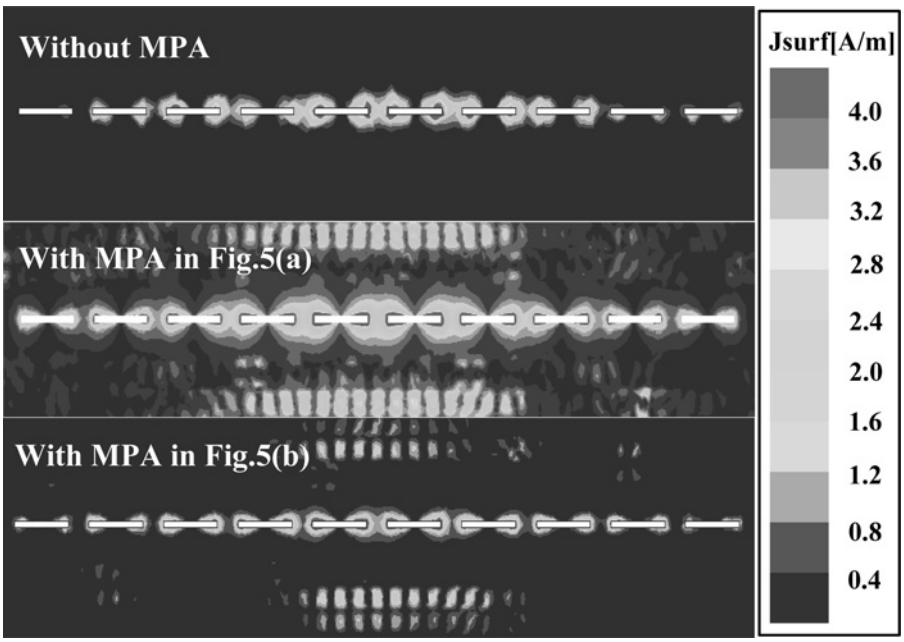

Fig. 8 *Surface current distributions of the antennas radiation without MPA and with MPA in Figs. 5a and b at 3.18 GHz*

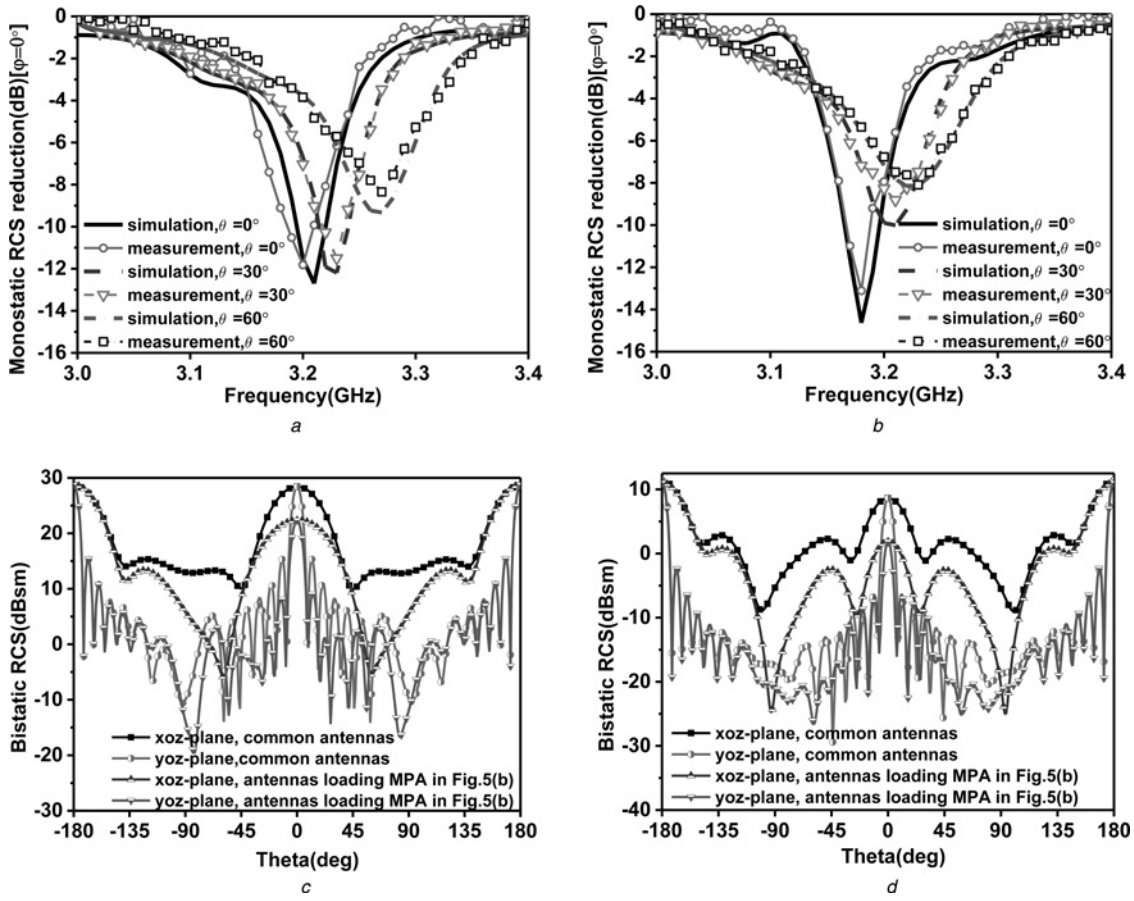

Fig. 9 *Comparison of monostatic and bistatic RCS for the guidewave slot array antennas loading MPA in Fig. 5b and common antennas*

Simulated and measured monostatic RCS reduction for
a *x*-polarised incident wave
b *y*-polarised incident wave with different incidence
Bistatic RCS for antennas loading MPA in Fig. 5*b* with
c *x*-polarised
d *y*-polarised incident wave at 3.18 GHz

than that for *x*-polarised incident wave. It can be explained by the periodic array theory that there are 44 MPA cells in the *y*-direction but 2 or 3 cells in the *x*-direction. The RCS can be reduced because of the surface current distributions of the antennas scatter without and with MPA at 3.18 GHz in Fig. 10. From Fig. 10, the current for the antennas without

© The Institution of Engineering and Technology 2015

doi: 10.1049/iet-map.2014.0490

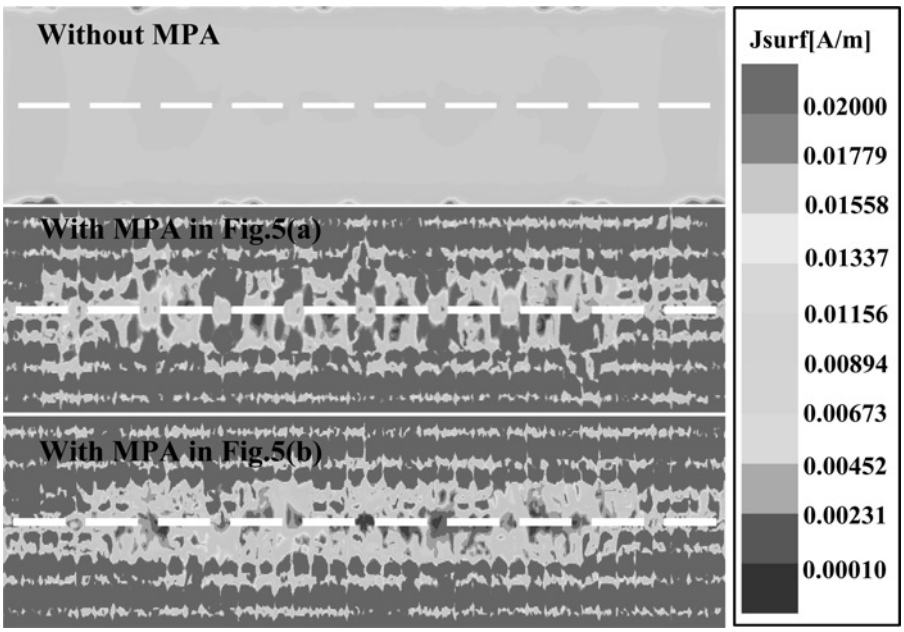

Fig. 10 *Surface current distributions of the antennas scatter (a) without MPA, (b) with MPA in Figs. 5a and c with MPA in Fig. 5b at 3.18 GHz*

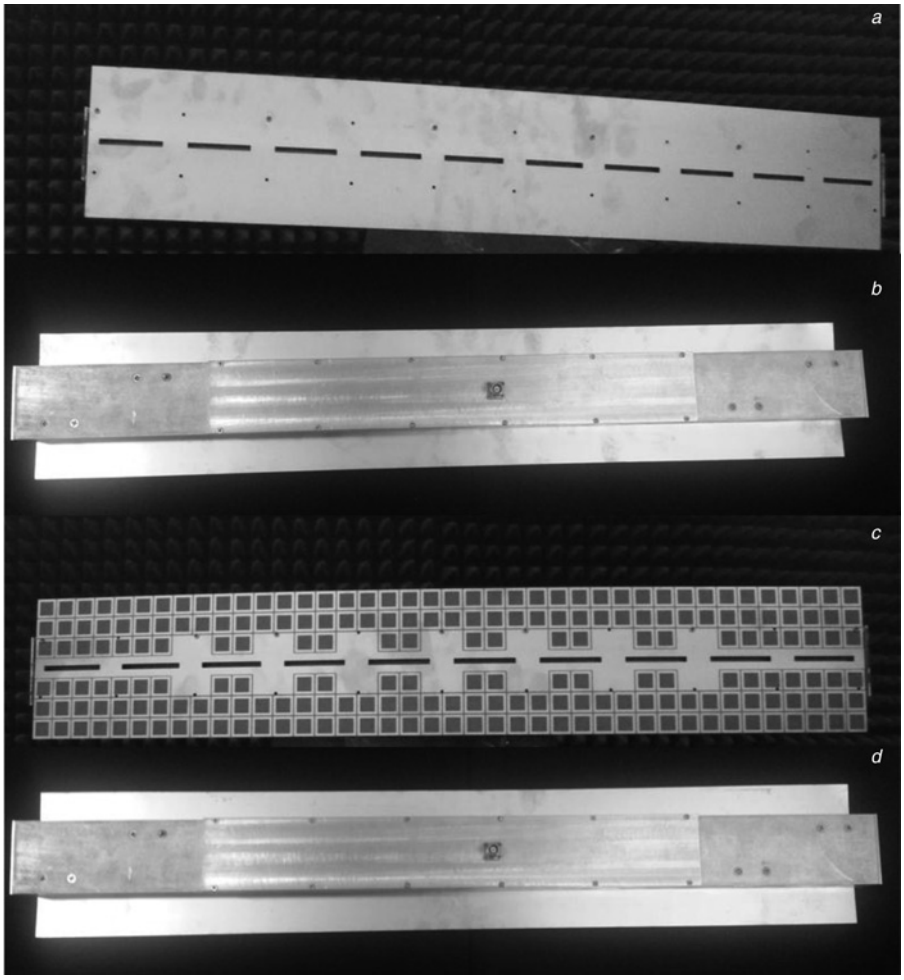

Fig. 11 *Prototypes of array antennas*

a Top view
b Bottom view of the proposed guidewave slot array antennas loading the MPA in Fig. 5*b*
c Top view
d Bottom view of the common array antennas

© The Institution of Engineering and Technology 2015

MPA distributes the entire metal plane. When the array antennas loaded the MPA, the surface current mainly distributes the area loading the three layers MPA which is caused by the absorption of the absorber.

4 Fabrication and measurement

To verify the simulation, the prototypes of the proposed guidewave slot array antennas loading the MPA in Fig. 5*b* and the common array antennas are illustrated in Fig. 11 and have been experimentally studies. The three layers MPA samples were, respectively, fabricated using an optical lithographic processes on a 0.3-mm-thick FR4 substrate with $\varepsilon_r = 4.4$ and $\tan\delta = 0.02$. The waveguide method [14–16] (closed system) has been used to verify the absorption. The measured results are shown in Fig. 1*b*. The measured absorptivity larger than 90% is ranging from 3.13 to 3.24 GHz with a FWHM of 136 MHz (3.134–3.27 GHz).

The experimental S_{11} and gain are given in Fig. 6. As seen from the curve, the antenna has a narrow impedance bandwidth of 2.5% from 3.15 to 3.23 GHz. The proposed array antennas obtain an average gain value of 13 dBi across the operating bandwidth from 3.15 to 3.23 GHz and the gain reduction is less than 0.73 dB. The experimental results indicate that the reliability of the loading MPA method for array RCS reduction based on its surface current distribution. Fig. 7*b* shows the experimental results at 3.18 GHz for both the *xoz*-plane and the *yoz*-plane. The patterns are stable across the operating bandwidth. The FBR remains to be better than 10.5 dB for the antennas loading MPA, which is 0.9 dB lower than that of common antennas.

The measured results of the monostatic RCS reduction for the array antennas are shown in Figs. 9*a* and *b*. The array antennas samples, respectively, have the monostatic RCS reduction peaks of −11.8 dB for 0° of incident angle and −8.1 dB for 60° of incident angle with *x*-polarised incident wave. The in-band RCS reduction peaks decreased from −13.1 to −8 dB for *y*-polarised incident wave, as the incident angle increased from 0° to 60°. The out-of-band RCS reduction is weaker than that of in-band. It is necessary to note that the resonant frequency will increase for the increase of the incident angle. The experimental results demonstrate that the array antennas loading MPA significantly obtains the in-band RCS reduction from 3.15 to 3.25 GHz for both the *x*-polarised and the *y*-polarised incident wave. In out-of-band, the radiation characters of the array antennas loading the three layers MPA are unchanged and the scatter characters are not significant. The experimental and simulated results are in good agreement.

5 Conclusion

In this paper, a loading MPA method is introduced to reduce the in-band RCS for guidewave slot array antennas and preserve the radiation characters. The surface current distributions of the array antennas divided into the strong and weak current areas are presented. The MPA is only loaded on the weak current area. The in-band RCS of the 1×10 guidewave slot array antennas is remarkably reduced using the method. Simulated *S*-parameter, radiation patterns, gain, directivity and in-band RCS reduction of the array are compared with the experimental results. Measured results indicated that the in-band RCS of the array antennas loading the MPA with the method has dramatically reduced than the common array antennas and the gain reduction is only about 0.73 dB. Experimentally and theoretically, it can be observed that the proposed method has the advantages of the low gain reduction and the high RCS reduction. Moreover, the next work is to enhance the absorption bandwidth of the metamaterial absorber.

6 Acknowledgments

Authors thank the supports from the National Natural Science Foundation of China under Grant (No. 61271100) and (No. 61471389), the Natural Science Foundational Research Fund of Shannxi Province (No. 2010JZ6010) and (No. 2012JM8003), and the Doctoral Foundation Air Force Engineering University under Grant (No. KGD080914002). They also thank the reviewers for their valuable comments.

7 References

1 Genovesi, S., Costa, F., Monorchio, A.: 'Wideband radar cross section reduction of slot antennas arrays', *IEEE Trans. Antennas Propag.*, 2014, **62**, (1), pp. 163–173
2 Pan, W., Huang, C., Chen, P., Ma, X., Hu, C., Luo, X.: 'A low-RCS and high-gain partially reflecting surface antenna', *IEEE Trans. Antennas Propag.*, 2014, **62**, (2), pp. 945–949
3 Zhou, H., Qu, S.-B., Lin, B.-Q.: 'Filter-antenna consisting of conical FSS radome and monopole antenna', *IEEE Trans. Antennas Propag.*, 2012, **60**, (6), pp. 3040–3045
4 Li, Y.-Q., Zhang, H., Fu, Y.-Q., Yuan, N.-C.: 'RCS reduction of ridged waveguide slot antenna array using EBG radar absorbing material', *IEEE Antennas Wirel. Propag. Lett.*, 2008, **7**, pp. 473–476
5 Tan, Y., Yan, N., Yang, Y., Fu, Y.: 'Improved RCS and efficient waveguide slot antenna', *Electron. Lett.*, 2011, **47**, (10), pp. 582–583
6 Zhang, Y., Mittra, R., Wang, B.-Z., Huang, N.T.: 'AMCs for ultra-thin and broadband RAM design', *Electron. Lett.*, 2009, **45**, (10), pp. 484–485
7 Hwang, R.B., Tsai, Y.L.: 'The reflection characteristics of a composite planar AMC surface', *AIP Advances*, 2012, **2**, (1), pp. 012128
8 Zhao, Y., Cao, X.Y., Gao, J., Li, W.Q.: 'Broadband RCS reduction and high gain waveguide slot antenna with orthogonal array of CSRR-AMC', *Electron. Lett.*, 2013, **49**, (21), pp. 1312–1313
9 Landy, N.I., Sajuyigbe, S., Mock, J.J., Smith, D.R., Padilla, W.J.: 'A perfect metamaterial absorber', *Phys. Rev. Lett.*, 2008, **100**, pp. 207402
10 Shen, X., Cui, T.J., Zhao, J., Ma, H., Jiang, W., Li, H.: 'Polarization-independent wide-angle triple-band metamaterial absorber', *Opt. Express*, 2011, **19**, (10), pp. 9401–9407
11 Wang, B.-X., Wang, L.-L., Wang, G.-Z., Huang, W.-Q., Li, X.-F., Zhai, X.: 'Theoretical investigation of broadband and wide-angle terahertz metamaterial absorber', *IEEE Photonics Technol. Lett.*, 2014, **26**, (2), pp. 111–114
12 Liu, T., Cao, X.Y., Gao, J., Zheng, Q.R., Li, W.Q., Yang, H.H.: 'RCS reduction of waveguide slot antenna with metamaterial absorber', *IEEE Trans. Antennas Propag.*, 2013, **61**, (4), pp. 2327–2335
13 Li, S.-J., Cao, X.-Y., Liu, T., Yang, H.-H.: 'Double-layer perfect metamaterial absorber and its application for RCS reduction of antenna', *Radio Eng.*, 2014, **23**, (1), pp. 222–228
14 Li, L., Yang, Y., Liang, C.: 'A wide-angle polarization-insensitive ultra-thin metamaterial absorber with three resonant modes', *J. Appl. Phys.*, 2011, **110**, pp. 063702
15 Xu, W., Sonkusale, S.: 'Microwave diode switchable metamaterial reflector/absorber', *Appl. Phys. Lett.*, 2013, **103**, pp. 0301902
16 Li, S.-J., Gao, J., Cao, X.-Y., Zhang, Z.: 'Loaded metamaterial perfect absorber using substrate integrated cavity', *J. Appl. Phys.*, 2014, **115**, pp. 213703
17 Li, S.-J., Gao, J., Cao, X.-Y., Li, W., Zhang, Z., Zhang, D.: 'Wideband, thin and polarization-insensitive perfect absorber based the double octagonal rings metamaterials and lumped resistances', *J. Appl. Phys.*, 2014, **116**, pp. 043710

© The Institution of Engineering and Technology 2015

doi: 10.1049/iet-map.2014.0490

Copyright of IET Microwaves, Antennas & Propagation is the property of Institution of Engineering & Technology and its content may not be copied or emailed to multiple sites or posted to a listserv without the copyright holder's express written permission. However, users may print, download, or email articles for individual use.